Appl. Math. Mech. -Engl. Ed., **47**(5), 1001–1018 (2026)

APPLIED MATHEMATICS AND MECHANICS (ENGLISH EDITION)

https://doi.org/10.1007/s10483-026-3379-9

Adhesion of stretched elastomers: a model based on Lennard-Jones potential*

Le DU[1], Jianmin LONG[2], Zhaohe DAI[3], Rui XIAO[1,†], Weiqiu CHEN[1]

1. Department of Engineering Mechanics, Zhejiang University, Hangzhou 310027, China;
2. College of Mechanics and Engineering Science, Hohai University, Nanjing 210098, China;
3. School of Mechanics and Engineering Science, Peking University, Beijing 100871, China

(Received Dec. 29, 2025 / Revised Mar. 4, 2026)

Abstract Pre-strain and pre-stress in soft materials have significant effects on their adhesive behavior, thereby influencing their functions and applications. Whereas prior theoretical studies on the adhesion of pre-strained elastomers predominantly rely on fracture mechanics frameworks based on the assumption of short-range forces, this study models surface interactions using the Lennard-Jones potential, thereby elucidating more intricate details of the adhesive behavior. The results of the proposed model are initially validated through finite element simulations and the analytical models in the literature. Subsequently, the effects of substrate pre-stretch on the adhesive behavior, including the pull-off force, JKR-Bradley transition, jump-in and jump-out instabilities, surface profile, and pressure distribution, are revealed by the proposed model. Based on the 'semi-rigid' theory (SRT), an analytical solution is derived to predict the displacement and central gap at the jump-in point. A modified Tabor parameter that incorporates the substrate pre-stretch effect is also proposed. The JKR-Bradley transition characterized by this modified parameter coincides with the unstretched case. This study offers new insights into understanding the adhesive behavior of pre-stretched elastomers.

Key words adhesion, Lennard-Jones potential, pre-stretch, pull-off force, jump-in/out instabilities, Tabor parameter

Chinese Library Classification O343.3
2020 Mathematics Subject Classification 74M15

1 Introduction

Surface adhesion widely exists in both engineering applications and biological systems[1–2]. For example, it plays a pivotal role in manipulating micro/nano-particles using an atomic force microscope (AFM)[3–4], designing advanced and smart adhesive materials[5–6], realizing soft robotic gripping[7], enabling geckos and spiders to adhere to and move across diverse surfaces

* Citation: DU, L., LONG, J. M., DAI, Z. H., XIAO, R., and CHEN, W. Q. Adhesion of stretched elastomers: a model based on Lennard-Jones potential. *Applied Mathematics and Mechanics* (*English Edition*), **47**(5), 1001–1018 (2026) https://doi.org/10.1007/s10483-026-3379-9

† Corresponding author, E-mail: rxiao@zju.edu.cn

Project supported by the National Natural Science Foundation of China (No. 12321002) and the 111 Project of China (No. B21034)

©Shanghai University 2026

with their feet and setae[8–9], as well as in surgical tapes for wound closure[10]. The pioneering research on adhesion can be traced back to Bradley[11], who first studied how two rigid spheres adhere to one another by applying the Lennard-Jones potential. Johnson, Kendall, and Roberts further took adhesive (van der Waals) forces into account in contact mechanics. By extending Hertz's solution[12] for the contact of two elastic spheres and utilizing the global energy balance method, they developed the classical JKR theory[13]. Later, in 1975, Derjaguin, Muller, and Toporov proposed another classical adhesion model, the DMT model[14], under the assumption that attractive forces act only beyond the contact zone and do not affect the deformation of the spheres. The divergence in the pull-off force estimations between the JKR and DMT frameworks led to intense debate, which was eventually settled by Tabor[15] through the proposal of a non-dimensional parameter, expressed as

$$\mu^* = \Big(\frac{R\Delta\gamma^2}{E^{*2}z_0^3}\Big)^{1/3}, \tag{1}$$

where R stands for the radius of the sphere, $\Delta\gamma$ characterizes the interfacial energy, E^* denotes the effective elastic modulus, and z_0 corresponds to the atomic equilibrium distance. It is now well established that the JKR theory is applicable to cases with large Tabor numbers, while the DMT/Bradley framework is more appropriate when the Tabor parameter takes small values. Maugis[16] used the Dugdale model[17] to describe surface interactions, treating the attractive force within the adhesive zone beyond the contact region as uniform. An analytical solution was derived, providing a smooth transition between the JKR and DMT models.

Recently, there has been a surge of focus on adhesive contact mechanics, with specific emphasis on soft materials such as rubbers, gels, and biological tissues. These materials often exhibit low elastic moduli and are capable of sustaining finite pre-stretch or pre-strain without failure[18–19], and generally allow a larger interaction area to fall within the range of adhesive forces[20]. Earlier studies have revealed that the presence of pre-strain and pre-stress in such soft materials is commonplace and can significantly influence their performance and functionality[21–26]. However, the question of how the presence of pre-strain and pre-stress in soft materials affects their adhesive behavior still remains largely unsolved.

Experimentally, an important observation is that when a spherical indenter and a cylindrical indenter come into adhesive contact with a substrate that has been equally biaxially stretched, the contact area decreases as the degree of substrate stretch increases[27–28]. Frétigny and Chateauminois[29] and Barney and Zheng[30] conducted a series of experiments to explore the adhesion of a rigid spherical indenter on elastomers that had been non-equally biaxially pre-stretched. Frétigny and Chateauminois focused on the long-term development of the elliptical contact region, while Barney and Zheng concentrated on its instantaneous evolution. Theoretically, since the mechanical behavior of soft materials may significantly deviate from the assumptions of linear elasticity, He and Ding[31] investigated the adhesion of a spherical indenter and an equally biaxially pre-stretched substrate occupying a half-space based on the global energy method (JKR theory) combined with the surface Green's function derived from an incompressible neo-Hookean model[32]. They predicted that the pull-off force would remain unaffected by the stretching. Using the same surface Green's function proposed by He[32], Frétigny and Chateauminois[29] and Barney and Zheng[30] carried out theoretical investigations on the adhesion between a rigid spherical indenter and a non-equally biaxially pre-stretched substrate, with the key distinction that they assumed different pressure distributions. In addition, Zheng et al.[33] and Xia[34] studied adhesive contact problems in constrained swelling hydrogels and constrained electroactive gels, respectively, which require more specific and complex constitutive models to describe their mechanical behavior. By applying the theory of mixed-mode interfacial fracture, Argatov and Papangelo[35] investigated the case of post-adhesion substrate stretching subject to a no-slip constraint. They revealed that the applied stretch drives a con-

tinuous transition from the JKR curve to the Hertzian curve, which in turn diminishes the pull-off force.

Both experimental and theoretical studies have made valuable contributions to the understanding of the adhesive contact behavior of pre-stretched elastomers. However, the theoretical studies mentioned above were conducted using global or local energy balance approaches. These approaches account only for short-range intermolecular forces confined within the contact region, serving as approximations of the physical reality. In reality, when two objects come into adhesive contact, the surface interactions are long-range, and the corresponding Tabor parameter may have arbitrary values. However, the full self-consistent model (FSCM) based on the van der Waals force has successfully characterized the transition between the JKR and Bradley/DMT limits[36–39], and is regarded as the most accurate model within the scope of continuum mechanics[40]. More recently, the FSCM has been applied to study the effect of surface tension on the adhesive contact[41] and to analyze the adhesion behavior in a graded elastic substrate[40]. These advances have motivated us to employ the FSCM to investigate the adhesive contact of pre-stretched elastomers.

This study extends a self-consistent model based on the Lennard-Jones potential to study the adhesive contact of pre-stretched elastomers. The remainder of this paper is organized as follows. Section 2 provides a brief introduction of the surface Green's function for a pre-stretched incompressible neo-Hookean elastomer[32] and presents a mathematical description of the current problem. Section 3 presents validation and discussion of the results. Finally, concluding remarks are presented in Section 4.

2 Model formulation

We study the adhesive interaction between a rigid sphere with radius R and an elastomer characterized by an incompressible neo-Hookean model and subject to equibiaxial pre-stretch, as depicted in Fig. 1. The surface interactions are considered to be long-range and follow the Lennard-Jones potential. The elastomer occupies the half-space $z \leqslant 0$ and is equally biaxially stretched in the plane perpendicular to the z-axis, with a principal stretch λ. The elastomer has a shear modulus μ. The rigid sphere is assumed to move along the z-axis.

We make the following assumptions. First, the adhesive contact of the rigid sphere with the pre-stretched elastomer is frictionless. Second, the deformations induced by adhesion are small such that they can be linearly superimposed. Third, the surface energy of the incompressible pre-stretched elastomer is assumed strain-independent. The motivation for this assumption is as follows: the elastomers exhibit a solid-like behavior at the macroscopic scale, while retaining liquid-like characteristics at the microscopic scale[42]. The stretching of elastomers does not suppress the fluctuations of monomer positions, enabling monomers within the bulk to migrate to the surface of the stretched elastomers. Therefore, the energetic cost of creating a unit area of the elastomer surface is strain-independent[43]. This view is supported by a recent numerical study[44]. Furthermore, experimental evidence from the contact angle measurements by Schulman et al.[45] directly demonstrated that the surface energy of incompressible amorphous elastomers is strain-independent.

As the rigid sphere approaches the elastomer, the interfacial separation $h(r)$ between the two objects can be written as

$$h(r) = -\alpha + z_0 + \frac{r^2}{2R} + w(r), \tag{2}$$

where z_0 is the equilibrium distance between the two flat and parallel surfaces, in which the van der Waals force vanishes. The term α represents the vertical displacement of the indenter with respect to $z = -z_0$. The function $w(r)$ denotes the normal surface displacement of the

pre-stretched elastomer. According to the coordinate system convention, the values of α and $w(r)$ are negative in the upward vertical direction.

For an elastomer subject to biaxial stretching, He and Ding[31] provided a fundamental solution for incremental surface deformation. A polar coordinate system is defined in the x_1x_2-plane (perpendicular to the z-axis), with its center at the axis of symmetry, as illustrated in Fig. 2. θ is defined as the angle between the line connecting a surface point to the origin and the x_1-axis. Under the equibiaxial stretching of the elastomer described by the incompressible neo-Hookean model, a unit normal load at a surface point $\boldsymbol{\xi}$ generates a normal displacement $g(l)$ at position $\boldsymbol{x}$, which can be expressed as

$$g(l) = \frac{h^*(\lambda)}{2\pi\mu l}, \tag{3}$$

where $l = (r^2 + t^2 - 2rt\cos\theta)^{1/2}$ is the distance between $\boldsymbol{x}$ and $\boldsymbol{\xi}$, and t is the radial distance from $\boldsymbol{\xi}$ to the origin. The term $h^*(\lambda)$ is defined as[31]

$$h^*(\lambda) = \frac{\lambda^4(\lambda^3+1)}{\lambda^9+\lambda^6+3\lambda^3-1}. \tag{4}$$

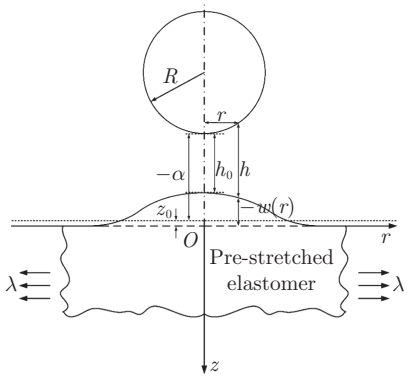

Fig. 1 Adhesive contact of a rigid spherical indenter with a pre-stretched elastomer, where the radius of the rigid sphere is R, and the principal stretch of the elastomer is λ

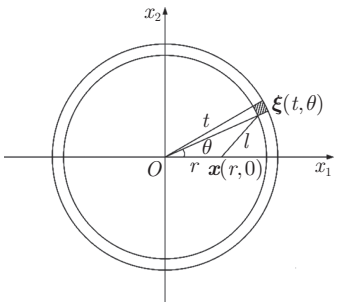

Fig. 2 Schematic diagram of the contact interface

Equations (3) and (4) provide the surface Green's function for the elastomer in its pre-stretched configuration. Under the assumption that the displacements induced by adhesion are small, the incremental displacement field on the surface of the pre-stretched elastomer can be obtained through linear superposition. The infinitesimal area element at point $\boldsymbol{\xi}$ is $t\mathrm{d}\theta\mathrm{d}t$. Given a specified pressure distribution $p(t)$, the surface displacement $w(r)$ at position $\boldsymbol{x}$ can be obtained using the surface integral of the product $p(t)g(l)$,

$$w(r) = \int_0^{2\pi}\int_0^{\infty} p(t)g(l)t\mathrm{d}\theta\mathrm{d}t = \frac{2h^*(\lambda)}{\pi\mu}\int_0^{\infty} p(t)\frac{t}{r+t}K\Big(\frac{2\sqrt{rt}}{r+t}\Big)\mathrm{d}t, \tag{5}$$

where $K(k)$ is the complete elliptic integral of the first kind, with k being the modulus.

Here, we assume that the surface interaction follows the Derjaguin approximation[37,46–48], which assumes that the interaction force between curved and inclined surfaces can be approximated by that between flat and parallel surfaces. This force is considered to act solely in the axial direction, with the radial components neglected (hence, the contact is frictionless). The

Lennard-Jones potential is adopted to capture the adhesive behavior between the rigid sphere and the pre-stretched elastomer. Accordingly, the pressure distribution $p(r)$ can be expressed as[49]

$$p(r) = -\frac{8\Delta\gamma}{3z_0}\Big(\Big(\frac{z_0}{h(r)}\Big)^3 - \Big(\frac{z_0}{h(r)}\Big)^9\Big), \tag{6}$$

where $\Delta\gamma$ denotes the interface energy between the rigid sphere and the elastomer. Therefore, the total force acting on the rigid sphere can be expressed as

$$P = \int_0^\infty p(r)2\pi r\mathrm{d}r. \tag{7}$$

By substituting Eq. (6) into Eq. (5) and then the latter into Eq. (2), a closed-form self-consistent equation is derived for the current adhesive contact problem, where the interfacial separation $h(r)$ is an unknown function. The governing equation is expressed as follows:

$$h(r) = -\alpha + z_0 + \frac{r^2}{2R} - \frac{16h^*(\lambda)\Delta\gamma}{3\pi\mu z_0}\int_0^\infty \Big(\Big(\frac{z_0}{h(t)}\Big)^3 - \Big(\frac{z_0}{h(t)}\Big)^9\Big)\frac{t}{r+t}K\Big(\frac{2\sqrt{rt}}{r+t}\Big)\mathrm{d}t. \tag{8}$$

When $\lambda = 1$, we have $h^* = 1/2$. Owing to incompressibility, Poisson's ratio ν is 0.5. The effective elastic modulus is given by $E^* = E/(1-\nu^2)$, where E denotes the elastic modulus, and the shear modulus is expressed as $\mu = E/(2(1+\nu))$. Thus, we have $\mu = E^*/4$. Then, Eq. (8) can be reduced to

$$h(r) = -\alpha + z_0 + \frac{r^2}{2R} - \frac{32\Delta\gamma}{3\pi E^* z_0}\int_0^\infty \Big(\Big(\frac{z_0}{h(t)}\Big)^3 - \Big(\frac{z_0}{h(t)}\Big)^9\Big)\frac{t}{r+t}K\Big(\frac{2\sqrt{rt}}{r+t}\Big)\mathrm{d}t, \tag{9}$$

which corresponds to the classical self-consistent equation for the adhesive contact of a rigid sphere with an elastic half-space modeled as a linear elastic constitutive model (without pre-stretch)[36–37,50].

For the purpose of nondimensionalization, we define the following dimensionless parameters:

$$H = h/z_0 - 1, \tag{10}$$

$$A = \alpha/z_0, \tag{11}$$

$$\rho = r/\sqrt{Rz_0}, \tag{12}$$

$$\tau = t/\sqrt{Rz_0}. \tag{13}$$

With these parameter definitions, the self-consistent equation (see Eq. (8)) can be expressed in a dimensionless form as follows:

$$\begin{aligned} H(\rho) = &-A + \frac{1}{2}\rho^2 - \frac{64h^*(\lambda)}{3\pi}(\mu^*)^{3/2}\rho \\ &\times \int_0^\infty \Big(\Big(\frac{1}{H(\tau)+1}\Big)^3 - \Big(\frac{1}{H(\tau)+1}\Big)^9\Big)\frac{\tau/\rho}{1+\tau/\rho}K\Big(\frac{2\sqrt{\tau/\rho}}{1+\tau/\rho}\Big)\mathrm{d}(\tau/\rho), \end{aligned} \tag{14}$$

where $\mu^* = (R\Delta\gamma^2/(E^{*2}z_0^3))^{1/3}$ denotes the classical Tabor parameter, which characterizes the transition of the pull-off force for the adhesive contact of homogeneous linear elastic solids from the JKR limit[13] to the Bradley/DMT limit[11,14]. In this work, we propose a modified Tabor parameter μ_{mod} that accounts for the effect of the substrate pre-stretch, which is defined as

$$\mu_{\mathrm{mod}} = \Big(\frac{4h^*(\lambda)^2 R\Delta\gamma^2}{E^{*2}z_0^3}\Big)^{1/3} = (2h^*(\lambda))^{2/3}\mu^*. \tag{15}$$

Accordingly, Eq. (14) can be rewritten as

$$H(\rho) = -A + \frac{1}{2}\rho^2 - \frac{32}{3\pi}(\mu_{\mathrm{mod}})^{3/2}\rho \times \int_0^{\infty} \Big(\Big(\frac{1}{H(\tau)+1}\Big)^3 - \Big(\frac{1}{H(\tau)+1}\Big)^9\Big)\frac{\tau/\rho}{1+\tau/\rho}K\Big(\frac{2\sqrt{\tau/\rho}}{1+\tau/\rho}\Big)\mathrm{d}(\tau/\rho). \tag{16}$$

The solution to the present adhesion problem requires solving the nonlinear integral equation (see Eq. (16)). However, $K(2(\tau/\rho)^{1/2}/(1+\tau/\rho))$ in Eq. (16) exhibits a singularity when $\tau = \rho$[37]. Various approaches have been proposed to address this singularity[36–37,51]. In this study, we adopt the exact method developed by Zheng et al.[52], which introduces a function Ψ with s as the independent variable, defined as

$$\Psi(s) = \frac{1}{\pi}\Big((s-1)K\Big(\frac{2\sqrt{s}}{1+s}\Big) + (s+1)E\Big(\frac{2\sqrt{s}}{1+s}\Big)\Big) - s, \tag{17}$$

and its derivative with respect to s is given by

$$\frac{\mathrm{d}\Psi(s)}{\mathrm{d}s} = \frac{2s}{\pi(s+1)}K\Big(\frac{2\sqrt{s}}{1+s}\Big) - 1. \tag{18}$$

Although Eq. (18) exhibits a singularity as s approaches 1, Eq. (17) remains continuous within this limit. For comprehensive discussion, readers can refer to the studies by Zheng et al.[52] and Zhu et al.[40,53]. Accordingly, Eq. (16) can be rewritten in the following form:

$$H(\rho) = -A + \frac{1}{2}\rho^2 - \frac{16}{3}(\mu_{\mathrm{mod}})^{3/2}\rho \times \int_{\tau=0}^{\tau=\infty} \Big(\Big(\frac{1}{H(\tau)+1}\Big)^3 - \Big(\frac{1}{H(\tau)+1}\Big)^9\Big)(\mathrm{d}\Psi(\tau/\rho) + \mathrm{d}(\tau/\rho)). \tag{19}$$

By employing the Riemann-Stieltjes integral method in Eq. (19) for numerical calculations, the integral singularity can be eliminated[40,52–53]. As the rigid sphere approaches or retracts from the surface of the elastomer, it is often accompanied by an instant of abrupt surface contact (jump-in) or separation (jump-out)[3,54]. Therefore, in numerical calculations, the choice of an appropriate control scheme is crucial for obtaining a complete force-displacement curve. Due to the non-convergence issues of the displacement control method near jumping points and the high computational cost of the arc-length control method[40], the surface central gap control method is employed in this study. By setting $\rho = 0$, we can obtain the expression for the central gap $H(0)$ as follows:

$$H(0) = -A - \frac{16}{3}(\mu_{\mathrm{mod}})^{3/2}\int_0^{\infty} \Big(\Big(\frac{1}{H(\tau)+1}\Big)^3 - \Big(\frac{1}{H(\tau)+1}\Big)^9\Big)\mathrm{d}\tau. \tag{20}$$

Then, we can substitute A with an expression involving $H(0)$. Consequently, Eq. (19) can be rewritten as

$$H(\rho) = H(0) + \frac{1}{2}\rho^2 - \frac{16}{3}(\mu_{\mathrm{mod}})^{3/2}\rho\int_{\tau=0}^{\tau=\infty} \Big(\Big(\frac{1}{H(\tau)+1}\Big)^3 - \Big(\frac{1}{H(\tau)+1}\Big)^9\Big)\mathrm{d}\Psi(\tau/\rho). \tag{21}$$

For the sake of conciseness, a brief description of the numerical algorithm used to solve Eq. (21) and calculate the normalized displacement A and the normalized load $P/(\pi\Delta\gamma R)$ is presented in Appendix A.

3 Results and discussion

3.1 Model validation

In the numerical calculations, the number of segments N is set to 500 for most results, with a few cases using $N = 1\,600$ to address the convergence issues (when $\mu_{\mathrm{mod}} > 5$). To verify the correctness of the FSCM, finite element simulations are conducted. It is worth noting that in both finite element simulations and real experiments, displacement control is typically adopted rather than surface central gap control. For large Tabor numbers, hysteresis may occur. Therefore, finite element analysis may encounter severe convergence issues under such conditions. In this case, we compare the results of the FSCM with the analytical results of He and Ding[31].

The finite element simulations are conducted using the commercial software ABAQUS. A rigid sphere undergoes adhesive contact with the pre-stretched elastomer, as shown in Fig. 3. We apply the incompressible neo-Hookean model to characterize the mechanical behavior of the pre-stretched elastomer. The substrate consists of 37 330 four-node bilinear axisymmetric quadrilateral elements, with the mesh near the axis of symmetry refined to $0.001\,5R$. We set the normal displacement constraints at the axis of symmetry, as well as on the right side and bottom of the elastomer. Prior to adhesive contact, the elastomer undergoes pre-stretch, which introduces both pre-strain and pre-stress to the elastomer. Nonlinear connectors are used to model the adhesive force. Each connector is placed between the center of the rigid sphere and the surface node of the pre-stretched elastomer, providing a force only in the vertical direction. Based on the Lennard-Jones potential (see Eq. (6)), a connector attached to a surface node at a radial distance r from the axis of symmetry exerts an adhesive force as[54–55]

$$\mathrm{d}P(r) = p(r)2\pi r\mathrm{d}r = -\frac{16\pi r\Delta\gamma}{3z_0}\left(\left(\frac{z_0}{h(r)}\right)^3 - \left(\frac{z_0}{h(r)}\right)^9\right)\mathrm{d}r. \tag{22}$$

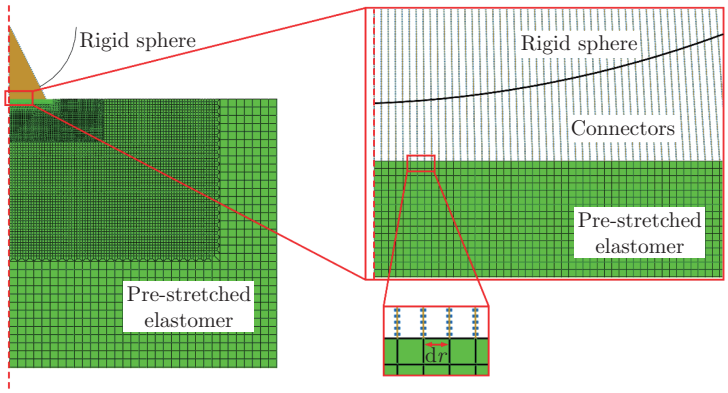

Fig. 3 Finite element model (FEM) of the adhesive contact between a rigid sphere and a pre-stretched elastomer with a detailed view of the interface (color online)

In the following comparison, we normalize P with respect to $\pi\Delta\gamma R$. We compare the FSCM results with the finite element results for low classical Tabor parameters ($\mu^* = 0.01,\ 0.3,\ 0.5$) and different substrate stretches ($\lambda = 0.8, 1$ (without stretch), 2), as shown in Figs. 4(a)–4(c). For the purpose of comparison, we also plot the Bradley curve[37], which is defined as

$$\frac{P}{\pi\Delta\gamma R} = \frac{2(1-4(1-A)^6)}{3(1-A)^8}. \tag{23}$$

It can be observed from Figs. 4(a)–4(c) that when the Tabor number is relatively small, i.e., $\mu^* = 0.01,\ 0.3,\ 0.5$, the results from the FSCM and the finite element simulations align

well under different stretching states. Moreover, the results for $\mu^* = 0.01$ nearly overlap with the Bradley curve, regardless of the stretching state. For the stretched substrate ($\lambda = 2$), the difference in the force-displacement curves due to variations in μ^* becomes smaller, while for the compressed substrate ($\lambda = 0.8$), the difference in the force-displacement curves due to variations in μ^* becomes larger. This suggests that stretching the substrate helps to resist adhesion-induced deformation, while compressing the substrate increases adhesion-induced deformation.

By employing the global energy balance method (JKR theory), He and Ding[31] provided an analytical solution for the adhesion of a rigid spherical indenter and a pre-stretched elastomer modeled as an incompressible neo-Hookean material and subject to equibiaxial stretching. The displacement and force are given as[31]

$$P = \frac{8\mu a^3}{3Rh} - 4\sqrt{\frac{\pi\mu\Delta\gamma a^3}{h^*(\lambda)}}, \tag{24}$$

$$\delta = \frac{a^2}{R} - \sqrt{\frac{\pi h^*(\lambda)\Delta\gamma a}{\mu}}, \tag{25}$$

where a stands for the contact radius between the rigid sphere and the pre-stretched elastomer. When the classical Tabor number is relatively large, i.e., $\mu^* = 5$, we compare the FSCM results with the analytical results from the JKR model[13] ($\lambda = 1$) and those from He and Ding[31] ($\lambda \neq 1$), as shown in Fig. 4(d).

Figure 4(d) indicates that the FSCM results align well with the analytical results in the high-force branch, whereas a discrepancy appears in the low-force branch. This is because the analytical model does not account for intermolecular forces as long-range interactions. In Fig. 4(d), we also mark the jump-in, jump-out, and pull-off points, which represent the onset of instabilities during the approach process, onset of instabilities during the retraction process, and location of the maximum attractive force, respectively. It can be seen that the JKR model[13] and the model proposed by He and Ding[31] effectively capture the jump-out and pull-off points. However, these models fail to capture the jump-in point.

3.2 Pull-off force and JKR-Bradley transition

In the study of the adhesive contact between a rigid sphere and a pre-stretched elastomer, the pull-off force, denoted as P_c, which is the maximum attractive force between the two objects, is of fundamental significance. It is well established that for small values of the classical Tabor parameter, the pull-off force approaches the Bradley limit, which corresponds to the minimum value in Eq. (23), i.e., $P_c/(\pi\Delta\gamma R) = -2$. For large values of the classical Tabor parameter, according to the result reported by He and Ding[31] (see Eq. (24)), the contact radius corresponding to the pull-off force, a^{pull}, can be obtained from the condition $\frac{\mathrm{d}P}{\mathrm{d}a} = 0$ as

$$a^{\text{pull}} = \Big(\frac{3}{4}\sqrt{\frac{\pi\Delta\gamma h^*}{\mu}}R\Big)^{2/3}. \tag{26}$$

By substituting the expression of a^{pull} into Eq. (24), the pull-off force can be calculated. After normalization by $\pi\Delta\gamma R$, we have $P_c/(\pi\Delta\gamma R) = -1.5$. Therefore, within the theoretical framework of He and Ding[31], the pull-off force does not vary with the pre-stretch λ applied to the elastomer, but remains consistent with the JKR model[13].

In Fig. 5, we depict the force-displacement curves at two representative classical Tabor parameters, $\mu^* = 1$ and $\mu^* = 5$, under different stretch states ($\lambda = 0.76, 0.8, 1, 2, 5, 10, 20$). The curves are compared with the Bradley curve in Figs. 5(a) and 5(b), as well as the JKR curve in Figs. 5(c) and 5(d). It should be noted that the values of λ representing compression cannot be arbitrarily chosen, as the critical conditions for Biot surface instability[56] and crease formation[19] occur at $\lambda^{3/2} = 0.543$ and $\lambda^{3/2} = 0.65$, respectively. Therefore, in this study, the

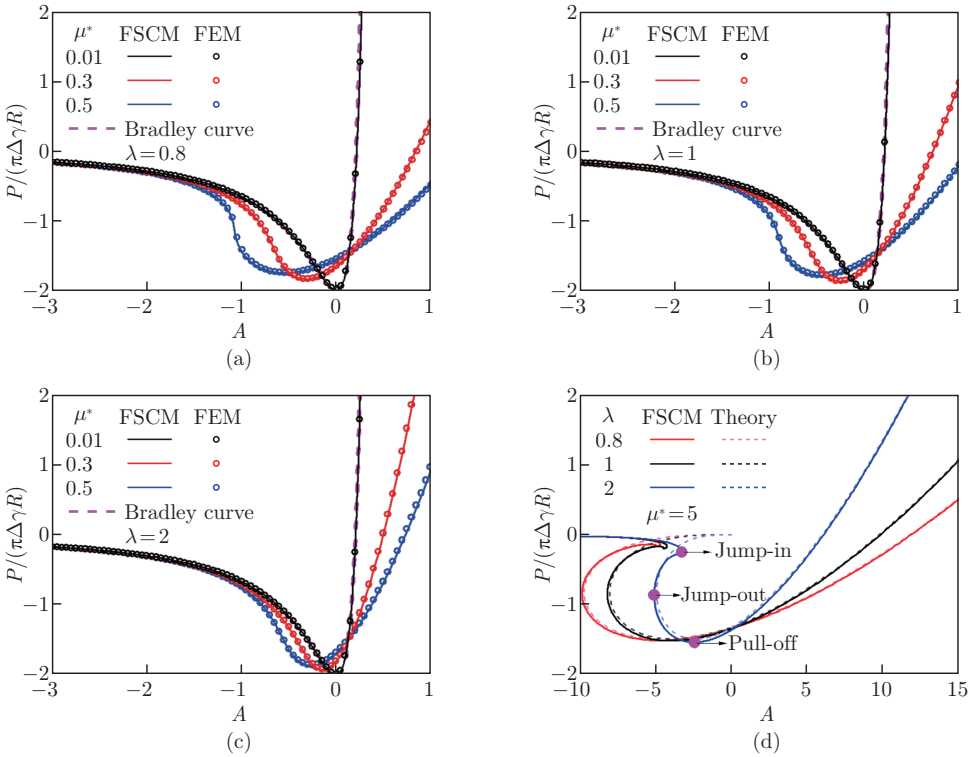

Fig. 4 (a)–(c) Comparison between the FSCM and finite element results for force-displacement curves at small classical Tabor numbers ($\mu^* = 0.01, 0.3, 0.5$) under different stretching states ($\lambda = 0.8$, 1, 2); (d) comparison between the FSCM and theoretical results at $\mu^* = 5$ under different stretching states ($\lambda = 0.8, 1, 2$), where the black dashed line is for the results from the JKR model[13], while the red and blue dashed lines are for the results from the model of He and Ding[31] (color online)

minimum compression value considered is $\lambda = 0.76$ to avoid crease formation. From Figs. 5(a) and 5(b), it can be seen that as the elastomer is stretched, the hysteresis phenomenon gradually disappears. For a large stretch (e.g., $\lambda = 20$), the force-displacement curve tends to approach the Bradley curve. This can be naturally understood, as the elastomer becomes stiffer due to the large stretch, resembling the adhesive contact between two rigid spheres. In contrast, when the elastomer is compressed, Figs. 5(c) and 5(d) show that the absolute value of the displacement at the jump-out point increases and the hysteresis phenomenon becomes more pronounced. The force-displacement curve does not further approach the JKR curve, but instead exceeds the envelope of the JKR curve.

Figure 6 provides more details on how the pull-off force varies with the pre-stretch and the Tabor parameter. From Fig. 6(a), it can be seen that, at a fixed classical Tabor parameter, the absolute value of the pull-off force P_c increases with the stretch ratio λ, indicating that separating the two bodies typically requires overcoming a larger detachment force. The effect of the classical Tabor parameter on the dimensionless pull-off force is examined for $\lambda = 0.8$, 1, 2, 3, as presented in Fig. 6(b). As the classical Tabor parameter increases from 0 to infinity, the pull-off force predicted by the FSCM transitions from the Bradley limit to the JKR limit. Moreover, the larger the stretch applied to the elastomer, the higher the pull-off force obtained at the same classical Tabor parameter. In addition, when the JKR-Bradley transition is characterized using the modified Tabor parameter μ_{mod} (see Eq. (15)), we can find that all curves converge to a single master curve, which is identical to the unstretched case, as shown in Fig. 6(c). This

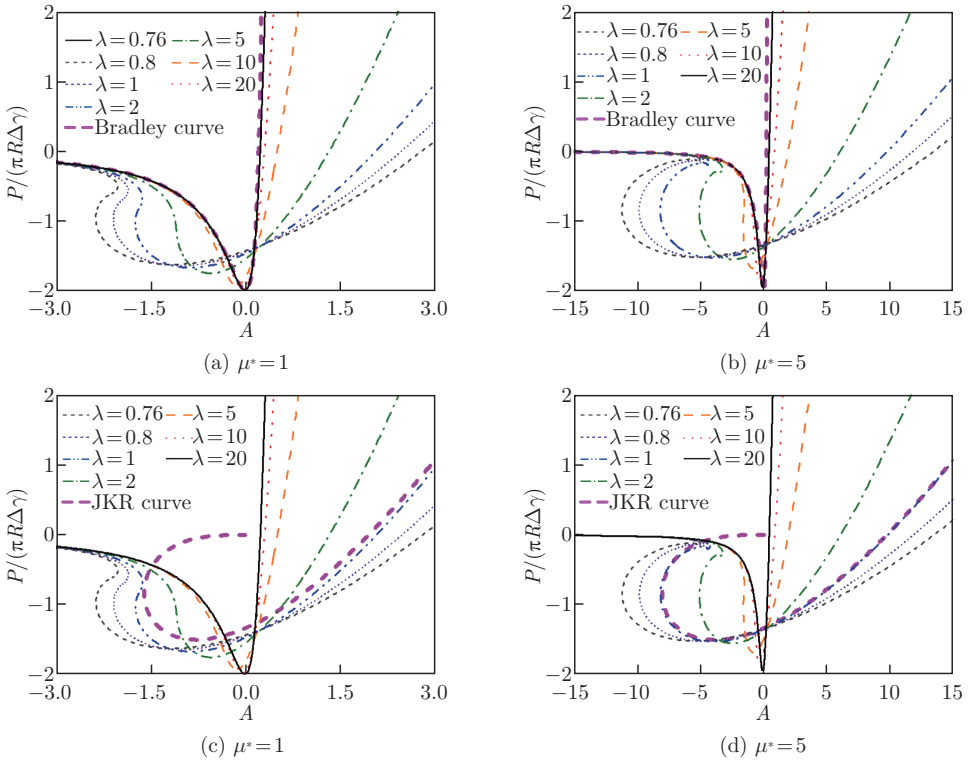

Fig. 5 Force-displacement curves for (a) and (c) $\mu^* = 1$ and (b) and (d) $\mu^* = 5$ under different stretching states ($\lambda = 0.76, 0.8, 1, 2, 5, 10,$ and 20), where (a) and (b) are compared with the Bradley curves, and (c) and (d) are compared with the JKR curves (color online)

indicates that the proposed modified Tabor parameter μ_{mod} is suitable for characterizing the adhesive contact behavior of pre-stretched substrates. Additionally, the JKR-DMT transition induced by stretching has recently been reported in thin-film systems[57–58], with conclusions similar to those of the current study, namely that the application of stretch can increase the absolute value of the pull-off force.

3.3 Jump-in and jump-out instabilities

Hysteresis occurs when the classical Tabor parameter is large, as the short-range component of intermolecular forces becomes dominant and is accompanied by energy dissipation during the approach and retraction cycles. In the preceding sections, we introduce the concepts of jump-in and jump-out points, as indicated in Fig. 4(d). By employing the FSCM presented in Section 2, we can directly extract the displacements at which jump-in and jump-out occur (A^{in} and A^{out}), as well as the corresponding surface separations at the symmetric center (H_0^{in} and H_0^{out}), under different stretching states and classical Tabor numbers, as shown in Figs. 7(a) and 7(b). As shown in Fig. 7(a), for all stretching states ($\lambda = 0.8, 1, 2, 3$), both the absolute values of A^{in} and A^{out} and their difference increase with the classical Tabor number. Figure 7(b) indicates that for all stretching states ($\lambda = 0.8, 1, 2, 3$), as the classical Tabor number increases, H_0^{in} and H_0^{out} exhibit increasing and decreasing trends, respectively. The intersection points of A^{in} and A^{out}, as well as H_0^{in} and H_0^{out}, define the critical classical Tabor parameter for the onset of hysteresis. The stretching of the elastomer ($\lambda > 1$) shifts the onset of hysteresis to larger classical Tabor numbers, whereas compression ($\lambda < 1$) promotes the onset of hysteresis to smaller classical Tabor numbers.

Although the jump-in and jump-out positions can be numerically extracted for arbitrary classical Tabor numbers and stretching states using the FSCM, an analytical solution is more

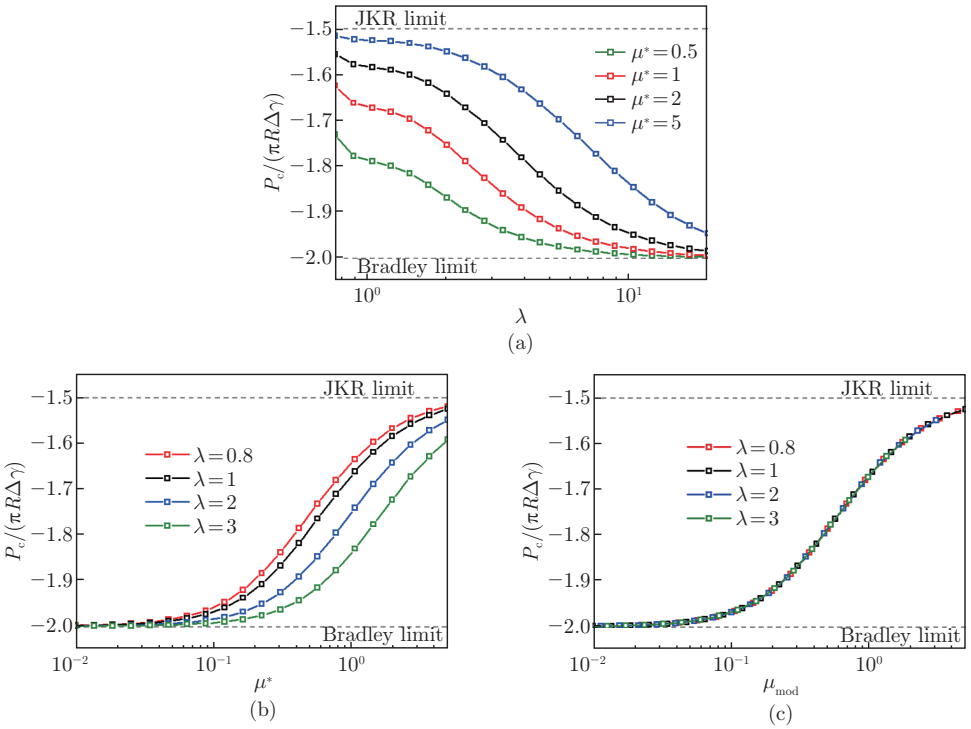

Fig. 6 (a) Normalized pull-off force as a function of the pre-stretch λ for different classical Tabor parameters ($\mu^* = 0.5, 1, 2, 5$); (b) normalized pull-off force as a function of the classical Tabor parameter μ^* for different pre-stretch values ($\lambda = 0.8, 1, 2, 3$); (c) normalized pull-off force as a function of the modified Tabor parameter $\mu_{\rm mod}$ for different pre-stretch values ($\lambda = 0.8, 1, 2, 3$) (color online)

convenient and readily generalizable. Therefore, we derive closed-form expressions for the central gap at the jump-in/out position based on the 'semi-rigid' theory (SRT)[48,54,59–60]. It is worth noting that when the classical Tabor number is not very large, the central gap at the jump-in position between the rigid sphere and the elastomer is relatively large and the intermolecular interaction force described by the Lennard-Jones potential (see Eq. (6)) is weak, leading to small surface deformations. Under these conditions, the SRT provides a reasonable approximation. Accordingly, the separation between the rigid sphere and the pre-stretched elastomer can be expressed as

$$h(r) = h_0 + \frac{r^2}{2R}, \tag{27}$$

where h_0 is the central gap, as illustrated in Fig. 1.

According to Eq. (5), the surface deformation at $r = 0$ can be written as

$$w(0) = \frac{h^*(\lambda)}{\mu} \int_0^\infty p(t)\mathrm{d}t. \tag{28}$$

Substituting Eq. (27) into Eq. (6) and then into Eq. (28) yields

$$w(0) = -\frac{8h^*(\lambda)\Delta\gamma}{3\mu z_0} \int_0^\infty \left(\left(\frac{z_0}{h_0 + t^2/(2R)} \right)^3 - \left(\frac{z_0}{h_0 + t^2/(2R)} \right)^9 \right) \mathrm{d}t. \tag{29}$$

As depicted in Fig. 1, we can obtain the following geometric relation at $r = 0$:

$$h_0 = -\alpha + z_0 + w(0). \tag{30}$$

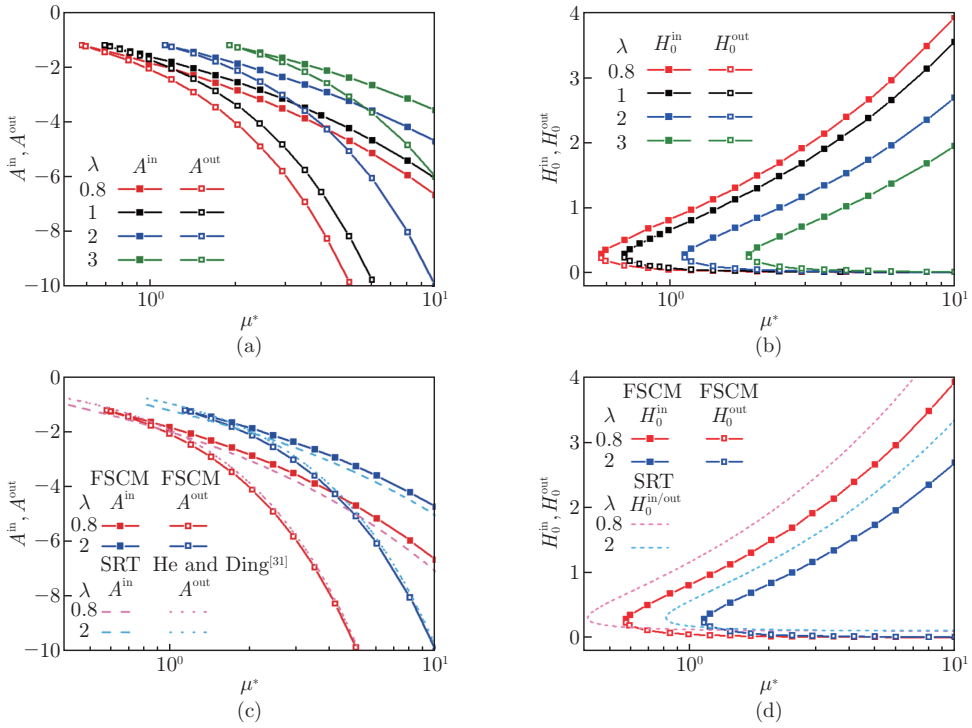

Fig. 7 (a) Displacement and (b) central gap at the jump-in and jump-out points as a function of the classical Tabor parameter for different pre-stretched states ($\lambda = 0.8, 1, 2, 3$); (c) comparison between the FSCM and analytical solutions (SRT and He and Ding[31]) for the displacement at the jump-in and jump-out points as a function of the classical Tabor parameter under different pre-stretches ($\lambda = 0.8, 2$); (d) comparison between the FSCM and analytical solutions (SRT) for the central gap at the jump-in and jump-out points as a function of the classical Tabor parameter under different pre-stretches ($\lambda = 0.8, 2$) (color online)

The jump-in and jump-out conditions should satisfy the following expressions[54]:

$$\frac{\mathrm{d}h_0}{\mathrm{d}\alpha} \to \infty \quad \text{or} \quad \frac{\mathrm{d}\alpha}{\mathrm{d}h_0} \to 0. \tag{31}$$

Taking the derivative of both sides of Eq. (30) with respect to h_0, we get

$$-\frac{\mathrm{d}\alpha}{\mathrm{d}h_0} = 1 - \frac{\mathrm{d}w(0)}{\mathrm{d}h_0}. \tag{32}$$

Therefore, the jump-in and jump-out conditions can be rewritten in the following mathematical form:

$$\frac{\mathrm{d}w(0)}{\mathrm{d}h_0} \to 1. \tag{33}$$

Based on the definitions of the dimensionless parameters H_0 and τ (see Eqs. (10) and (13)), and by substituting Eq. (29) into Eq. (33), we obtain the dimensionless criterion for the occurrence of jump-in and jump-out as

$$-\frac{16}{3}\mu_{\mathrm{mod}}^{3/2}\int_0^{\infty}\left(-3\left((H_0^{\mathrm{in/out}}+1)+\frac{\tau^2}{2}\right)^{-4}+9\left((H_0^{\mathrm{in/out}}+1)+\frac{\tau^2}{2}\right)^{-10}\right)\mathrm{d}\tau = 1. \tag{34}$$

After evaluating the integral in Eq. (34), it can be rewritten as

$$\frac{16}{3}\left(\frac{15\pi\sqrt{2}}{32}(H_0^{\mathrm{in/out}}+1)^{-7/2} - \frac{109\,395\pi\sqrt{2}}{131\,072}(H_0^{\mathrm{in/out}}+1)^{-19/2}\right) = \mu_{\mathrm{mod}}^{-3/2}. \tag{35}$$

When $\lambda = 1$, we have $h^* = 1/2$, and Eq. (35) reduces to the result reported by Song and Komvopoulos[54]. Once the central gap at the jump-in point, H_0^{in}, is obtained from Eq. (35), the corresponding jump-in displacement A^{in} can be estimated using Eqs. (29) and (30), as will be demonstrated below. Equation (29) can be reformulated in terms of the dimensionless quantities H_0^{in} and τ as

$$w(0) = -\frac{16z_0}{3}\mu_{\text{mod}}^{3/2}\int_0^{\infty}\left(\left((H_0^{\text{in}}+1)+\frac{\tau^2}{2}\right)^{-3}-\left((H_0^{\text{in}}+1)+\frac{\tau^2}{2}\right)^{-9}\right)\mathrm{d}\tau, \tag{36}$$

which can be reduced to the following expression by simplifying the integral:

$$w(0) = -\frac{16z_0}{3}\mu_{\text{mod}}^{3/2}\left(\frac{3\pi\sqrt{2}}{16}(H_0^{\text{in}}+1)^{-5/2}-\frac{6\,435\pi\sqrt{2}}{65\,536}(H_0^{\text{in}}+1)^{-17/2}\right). \tag{37}$$

Dividing both sides of Eq. (37) by z_0 gives us

$$\begin{aligned} A^{\text{in}} &= \frac{w(0)}{z_0} - H_0^{\text{in}} \\ &= -\frac{16}{3}\mu_{\text{mod}}^{3/2}\left(\frac{3\pi\sqrt{2}}{16}(H_0^{\text{in}}+1)^{-5/2}-\frac{6\,435\pi\sqrt{2}}{65\,536}(H_0^{\text{in}}+1)^{-17/2}\right) - H_0^{\text{in}}. \end{aligned} \tag{38}$$

So far, based on the SRT, we have obtained an estimation of the displacement at the jump-in point. However, for the jump-out point, the SRT is clearly no longer applicable, since the rigid sphere and the elastomer are at a critical state of separation, where the surface gap is extremely small. In this case, the analytical solution for pre-stretched elastomers proposed by He and Ding[31] provides a reliable prediction of the displacement at the jump-out point. The jump-out point can be determined by

$$\frac{\mathrm{d}\delta}{\mathrm{d}P} = \frac{\mathrm{d}\delta/\mathrm{d}a}{\mathrm{d}P/\mathrm{d}a} = 0. \tag{39}$$

As $\frac{\mathrm{d}P}{\mathrm{d}a}$ remains finite, the onset of jump-out is defined by the condition $\frac{\mathrm{d}\delta}{\mathrm{d}a} = 0$. Accordingly, with Eq. (25), we can obtain the radius of the contact region at the jump-out point a^{out} as

$$a^{\text{out}} = \left(\frac{\pi h^*(\lambda)\Delta\gamma R^2}{16\mu}\right)^{1/3}. \tag{40}$$

Then, by substituting the above expression of a^{out} into Eq. (25), the displacement corresponding to the jump-out point can be determined as

$$A^{\text{out}} = \frac{\delta(a^{\text{out}})}{z_0} = -\frac{3}{4}\pi^{2/3}\mu_{\text{mod}}. \tag{41}$$

Equation (41) indicates that A^{out} is proportional to μ_{mod}. When $\lambda = 1$ and $h^* = 1/2$, Eq. (41) reduces to the case without pre-stretch, which coincides with the homogeneous-material case of graded elastic materials reported by Zhu et al.[40]. The analytical solutions of H_0^{in}, H_0^{out}, and A^{in} derived from the SRT, together with the analytical solution of A^{out} obtained from the analytical solution proposed by He and Ding[31], are compared with those of the FSCM, as shown in Figs. 7(c) and 7(d). The analytical solutions of A^{in} and A^{out} show good agreement with the results of the FSCM. However, the analytical approach tends to underestimate the critical classical Tabor number at which jump-in/out occurs, as illustrated in Fig. 7(d).

3.4 Surface profile and pressure distribution

In this subsection, we investigate the surface profile and pressure distribution of the elastomer. For the surface profile, the deflection w of the elastomer surface is of greater interest and is more intuitive compared with the surface separation H. First, the surface separation is obtained using the FSCM. Then, based on the geometric relation in Eq. (2) and the dimensionless definitions in Eqs. (10)–(12), we have

$$-\frac{w}{z_0} = -A - H + \frac{\rho^2}{2}, \tag{42}$$

and for convenience, the following dimensionless pressure distribution is defined from Eqs. (6) and (10):

$$\frac{p}{\Delta\gamma/z_0} = -\frac{8}{3}((1+H(\rho))^{-3} - (1+H(\rho))^{-9}). \tag{43}$$

We focus on the case of $A = 0$, representing the condition in which two rigid spheres first make contact at a mathematical point[36]. The surface profile and the pressure distribution at $A = 0$ with $\mu^* = 1$ are shown in Figs. 8(a) and 8(b), respectively. Figure 8(a) presents the surface profile of the elastomer for different pre-stretch states ($\lambda = 0.8, 1, 2, 3$). The deformation of the elastomer surface decreases as the principal stretch λ increases. This intuitively reflects that stretching the elastomer helps it resist adhesion-induced deformation, whereas compression enhances such deformation. Figure 8(b) illustrates the corresponding pressure distribution of the elastomer surface. At the center of the contact region ($r/(Rz_0)^{1/2} = 0$), the interaction between the rigid sphere and the elastomer is repulsive. As $r/(Rz_0)^{1/2}$ increases, the interaction transitions to an attractive force, reaching a maximum absolute value corresponding to the theoretical strength of the Lennard-Jones potential, $-\sigma_{\rm th}$, which can be calculated from Eq. (6) as $-1.026\Delta\gamma/z_0$. This value is indicated by the gray dashed line in Figs. 8(b) and 8(d). As $r/(Rz_0)^{1/2}$ continues to increase, the attractive force decreases and approaches zero. With increasing pre-stretch, the position of $-\sigma_{\rm th}$ shifts closer to the axis of symmetry.

Figures 8(c) and 8(d) show the surface profile and pressure distribution for different pre-stretch states ($\lambda = 0.8, 1, 2, 3$) at $P/(\pi\Delta\gamma R) = 0$ with $\mu^* = 1$. At this stage, the rigid sphere and the elastomer are in equilibrium in the absence of an external load, with the attractive and repulsive forces of the intermolecular interactions balancing each other. From Fig. 8(c), it can be observed that the deflection of the elastomer surface is larger compared with the case of $A = 0$ (see Fig. 8(a)). Similarly, stretching the elastomer reduces deformation, while compression enhances it. Figure 8(d) shows that the minimum value $-\sigma_{\rm th}$ appears at a location farther away from the axis of symmetry, compared with the case of $A = 0$ (see Fig. 8(b)).

For the contact region, two definitions are commonly adopted[61]. One considers the contact region as the area where the pressure is positive, while the other defines it as the area enclosed by the peak tensile. If the second definition is adopted, Figs. 8(b) and 8(d) show that the contact region decreases with the increasing principal stretch λ of the elastomer. This observation is consistent with the conclusion of He and Ding[31].

4 Conclusions

Based on the Lennard-Jones potential law, we employ a numerical model to investigate the adhesion between a rigid spherical indenter and an elastomer subject to equibiaxial pre-stretch. In contrast to prior studies that assumed short-range adhesive forces, the present work models long-range intermolecular interactions, which more accurately reflects the physical reality and captures richer details of the adhesive process. A numerical algorithm is used to solve the nonlinear system of equations, which originates from a self-consistent equation describing the adhesive contact. For small classical Tabor parameters, the results from the FSCM and finite element simulations are in good agreement. At large classical Tabor parameters, we compare the FSCM results with previous theoretical models[13,31], which are consistent at higher forces.

The main findings are summarized as follows. First, the pre-stretching of the elastomer reduces the deformation induced by adhesion with a rigid sphere. The absolute value of the pull-off force between the rigid sphere and the pre-stretched elastomer increases with stretching, approaching the Bradley limit at extreme levels of stretch. In addition, based on the classical Tabor parameter, we introduce a modified Tabor parameter, which incorporates the effect of substrate pre-stretch. When the JKR-Bradley transition is characterized using this modified Tabor parameter, the curves for arbitrary pre-stretch collapse onto a single master curve that

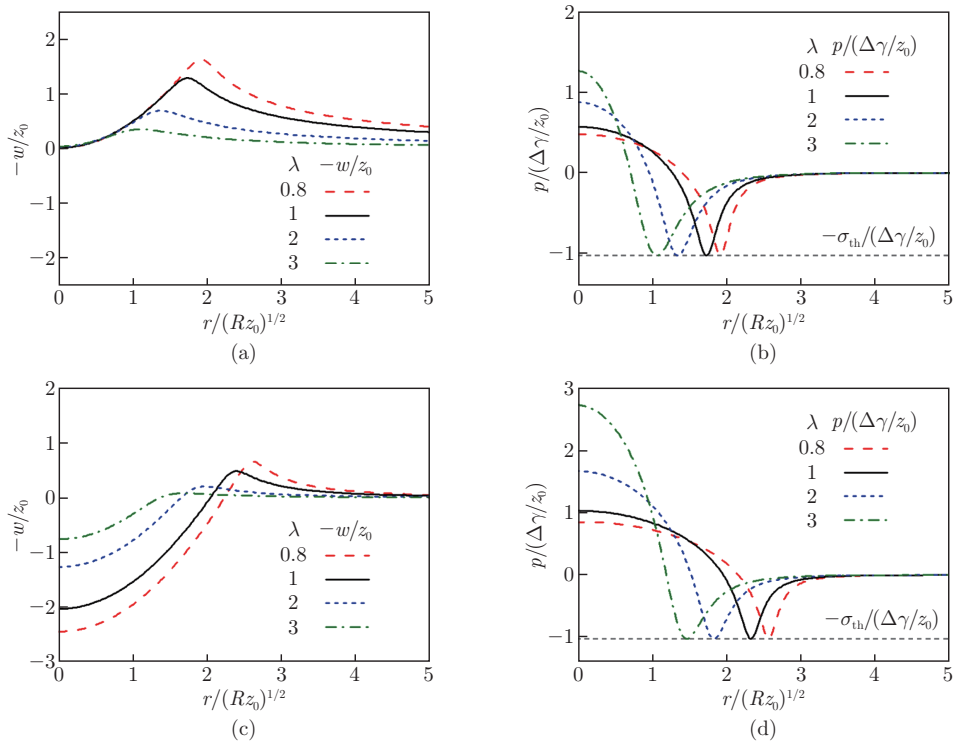

Fig. 8 Effects of the pre-stretch ($\lambda = 0.8, 1, 2, 3$) of the elastomer on (a) the surface profile and (b) the pressure distribution at $A = 0$ and $\mu^* = 1$ and effects of the pre-stretch ($\lambda = 0.8, 1, 2, 3$) of the elastomer on (c) the surface profile and (d) the pressure distribution at $P/(\pi\Delta\gamma R) = 0$ and $\mu^* = 1$ (color online)

coincides with the unstretched case. Finally, we analyze the hysteresis phenomena using both the FSCM and analytical approaches. Both sets of results indicate that stretching the elastomer shifts the onset of hysteresis to larger classical Tabor numbers. Overall, this study provides new insights into the adhesive contact of the pre-stretched elastomers. The work can be extended to the cases of indenters with other shapes and elastomers subject to unequibiaxial loading conditions.

Conflict of interest Weiqiu CHEN is an editorial board member for *Applied Mathematics and Mechanics* (*English Edition*) and was not involved in the editorial review or the decision to publish this article. The authors declare no conflict of interest.

References

[1] GAO, H. J. and YAO, H. M. Shape insensitive optimal adhesion of nanoscale fibrillar structures. *Proceedings of the National Academy of Sciences of the United States of America*, **101**(21), 7851–7856 (2004)

[2] SHULL, K. R. Contact mechanics and the adhesion of soft solids. *Materials Science and Engineering*: *R*: *Reports*, **36**(1), 1–45 (2002)

[3] DAI, Z. Jump of an atomic force microscopy probe towards an elastic substrate in a liquid environment. *Journal of Fluid Mechanics*, **1013**, A49 (2025)

[4] KIM, S., SHAFIEI, F., RATCHFORD, D., and LI, X. Q. Controlled AFM manipulation of small nanoparticles and assembly of hybrid nanostructures. *Nanotechnology*, **22**(11), 115301 (2011)

[5] ANNAPOORANAN, R., JEYAKUMAR, S. S., CHAMBERS, R. J., LONG, R., and CAI, S. Q. Ultra rate-dependent pressure sensitive adhesives enabled by soft elasticity of liquid crystal

elastomers. *Advanced Functional Materials*, **34**(1), 2309123 (2024)

[6] LEE, C., SHI, H. Q., JUNG, J., ZHENG, B. W., WANG, K., TUTIKA, R., LONG, R., LEE, B. P., GU, G. X., and BARTLETT, M. D. Bioinspired materials for underwater adhesion with pathways to switchability. *Cell Reports Physical Science*, **4**(10), 101597 (2023)

[7] YANG, X. W., SRIVASTAVA, A., and LONG, R. Adhesive contact of an inflated circular membrane with curved surfaces. *International Journal of Solids and Structures*, **279**, 112371 (2023)

[8] DONG, X. X., ZHANG, R., TIAN, Y., RAMOS, M. A., HU, T. S., WANG, Z. H., ZHAO, H., ZHANG, L. P., WAN, Y. Y., XIA, Z. H., and XU, Q. Functionally graded gecko setae and the biomimics with robust adhesion and durability. *ACS Applied Polymer Materials*, **2**(7), 2658–2666 (2020)

[9] FLENNER, S., SCHABER, C. F., KRASNOV, I., STIEGLITZ, H., ROSENTHAL, M., BURGHAMMER, M., GORB, S. N., and MÜLLER, M. Multiple mechanical gradients are responsible for the strong adhesion of spider attachment hair. *Advanced Materials*, **32**(37), 2002758 (2020)

[10] YUK, H., VARELA, C. E., NABZDYK, C. S., MAO, X. Y., PADERA, R. F., ROCHE, E. T., and ZHAO, X. H. Dry double-sided tape for adhesion of wet tissues and devices. *Nature*, **575**(7781), 169–174 (2019)

[11] BRADLEY, R. S. The cohesive force between solid surfaces and the surface energy of solids. *The London, Edinburgh, and Dublin Philosophical Magazine and Journal of Science*, **13**(86), 853–862 (1932)

[12] HERTZ, H. Ueber die Berührung fester elastischer Körper (on the contact of elastic solids). *Journal fur die Reine und Angewandte Mathematik*, **1882**(92), 156–171 (1882)

[13] JOHNSON, K. L., KENDALL, K., and ROBERTS, A. D. Surface energy and the contact of elastic solids. *Proceedings of the Royal Society of London. A: Mathematical and Physical Sciences*, **324**(1558), 301–313 (1971)

[14] DERJAGUIN, B. V., MULLER, V. M., and TOPOROV, Y. P. Effect of contact deformations on the adhesion of particles. *Journal of Colloid and Interface Science*, **53**(2), 314–326 (1975)

[15] TABOR, D. Surface forces and surface interactions. *Journal of Colloid and Interface Science*, **58**(1), 2–13 (1977)

[16] MAUGIS, D. Adhesion of spheres: the JKR-DMT transition using a Dugdale model. *Journal of Colloid and Interface Science*, **150**(1), 243–269 (1992)

[17] DUGDALE, D. S. Yielding of steel sheets containing slits. *Journal of the Mechanics and Physics of Solids*, **8**(2), 100–104 (1960)

[18] FUNG, Y. C. What are the residual stresses doing in our blood vessels? *Annals of Biomedical Engineering*, **19**(3), 237–249 (1991)

[19] HONG, W., ZHAO, X. H., and SUO, Z. G. Formation of creases on the surfaces of elastomers and gels. *Applied Physics Letters*, **95**(11), 111901 (2009)

[20] CIAVARELLA, M., JOE, J., PAPANGELO, A., and BARBER, J. R. The role of adhesion in contact mechanics. *Journal of the Royal Society Interface*, **16**(151), 20180738 (2019)

[21] CHATEAUMINOIS, A., NGUYEN, D. T., and FRÉTIGNY, C. Effects of stretching on the frictional stress of rubber. *Soft Matter*, **13**(35), 5849–5857 (2017)

[22] LIANG, T., YUAN, W. K., and WANG, G. F. Influence of equi-biaxial residual stress on spherical indentation of strain hardening materials. *International Journal of Applied Mechanics*, **13**(5), 2150052 (2021)

[23] RAUSCH, M. K. and KUHL, E. On the effect of prestrain and residual stress in thin biological membranes. *Journal of the Mechanics and Physics of Solids*, **61**(9), 1955–1969 (2013)

[24] ROGERS, J., HUANG, Y. G., SCHMIDT, O. G., and GRACIAS, D. H. Origami MEMS and NEMS. *MRS Bulletin*, **41**(2), 123–129 (2016)

[25] YUAN, L. X., YUAN, W. K., and WANG, G. F. Effects of residual stress on the hardness of elastoplastic material under spherical indentation. *Journal of Applied Mechanics*, **87**(5), 051004 (2020)

[26] ZHU, F. B., ZHANG, C. L., QIAN, J., and CHEN, W. Q. Mechanics of dielectric elastomers: materials, structures, and devices. *Journal of Zhejiang University: Science A*, **17**(1), 1–21 (2016)

[27] FELDER, E. and BARQUINS, M. Adherence of natural rubber plates subjected to biaxial tensile strain. *Journal of Physics D*: *Applied Physics*, **25**(1A), A9(1992)

[28] WATERS, J. F., KALOW, J., GAO, H. J., and GUDURU, P. R. Axisymmetric adhesive contact under equibiaxial stretching. *The Journal of Adhesion*, **88**(2), 134–144 (2012)

[29] FRÉTIGNY, C. and CHATEAUMINOIS, A. Contact of a spherical probe with a stretched rubber substrate. *Physical Review E*, **96**(1), 013001 (2017)

[30] BARNEY, C. W. and ZHENG, Y. L. Peeling a rigid sphere from a stretched rubber substrate. *Extreme Mechanics Letters*, **79**, 102381 (2025)

[31] HE, L. H. and DING, K. W. Adhesive contact of a rigid sphere to finitely stretched substrates. *Chinese Science Bulletin*, **54**(11), 1970–1972 (2009)

[32] HE, L. H. Elastic interaction between force dipoles on a stretchable substrate. *Journal of the Mechanics and Physics of Solids*, **56**(10), 2957–2971 (2008)

[33] ZHENG, Y., HU, Y. H., and CAI, S. Q. Contact mechanics of a gel under constrained swelling. *Journal of the Mechanics and Physics of Solids*, **124**, 427–445 (2019)

[34] XIA, G. Z. Indentation on a constrained electroactive gel. *Journal of the Mechanics and Physics of Solids*, **197**, 106045 (2025)

[35] ARGATOV, I. and PAPANGELO, A. Axisymmetric JKR-type adhesive contact under equibiaxial stretching. *The Journal of Adhesion*, **97**(2), 140–154 (2021)

[36] FENG, J. Q. Contact behavior of spherical elastic particles: a computational study of particle adhesion and deformations. *Colloids and Surfaces A*: *Physicochemical and Engineering Aspects*, **172**(1-3), 175–198 (2000)

[37] GREENWOOD, J. A. Adhesion of elastic spheres. *Proceedings of the Royal Society of London. Series A*: *Mathematical*, *Physical and Engineering Sciences*, **453**(1961), 1277–1297 (1997)

[38] YAN, S. P. and HE, L. H. Adhesive force between a spherical rigid particle and an incompressible elastic substrate. *Mechanics of Materials*, **49**, 66–71 (2012)

[39] YAN, S. P. and HE, L. H. Adhesive contact between a rigid nanofiber and an incompressible elastic substrate. *International Journal of Solids and Structures*, **50**(16-17), 2712–2717 (2013)

[40] ZHU, Y. D., ZHENG, Z. J., HUANG, C. G., and YU, J. L. Adhesion of graded elastic materials: a full self-consistent model and its application. *Journal of the Mechanics and Physics of Solids*, **169**, 105078 (2022)

[41] ZHU, X. Y. and XU, W. Effect of surface tension on the behavior of adhesive contact based on Lennard-Jones potential law. *Journal of the Mechanics and Physics of Solids*, **111**, 170–183 (2018)

[42] RUBINSTEIN, M. and PANYUKOV, S. Nonaffine deformation and elasticity of polymer networks. *Macromolecules*, **30**, 8036–8044 (1997)

[43] MASUREL, R., ROCHÉ, M., LIMAT, L., IONESCU, I., and DERVAUX, J. Elastocapillary ridge as a noninteger disclination. *Physical Review Letters*, **122**(24), 248004 (2019)

[44] LIANG, H. Y., CAO, Z., WANG, Z. L., and DOBRYNIN, A. V. Surface stress and surface tension in polymeric networks. *ACS Macro Letters*, **7**(1), 116–121 (2018)

[45] SCHULMAN, R. D., TREJO, M., SALEZ, T., RAPHAËL, E., and DALNOKI-VERESS, K. Surface energy of strained amorphous solids. *Nature Communications*, **9**, 982 (2018)

[46] DERJAGUIN, B. V. Theorie des anhaftens kleiner teilchen (theory of adhering small particles). *Kolloid-Zeitschrift*, **69**(2), 155–164 (1934)

[47] GREENWOOD, J. A. On the DMT theory. *Tribology Letters*, **26**(3), 203–211 (2007)

[48] GREENWOOD, J. A. Adhesion of small spheres. *Philosophical Magazine*, **89**(11), 945–965 (2009)

[49] ISRAELACHVILI, J. N. *Intermolecular and Surface Forces*, Academic Press, San Diego, CA (1992)

[50] MULLER, V. M., YUSHCHENKO, V. S., and DERJAGUIN, B. V. On the influence of molecular forces on the deformation of an elastic sphere and its sticking to a rigid plane. *Journal of Colloid and Interface Science*, **77**(1), 91–101 (1980)

[51] PAPANGELO, A. and CIAVARELLA, M. A numerical study on roughness-induced adhesion enhancement in a sphere with an axisymmetric sinusoidal waviness using Lennard-Jones interaction law. *Lubricants*, **8**(9), 90 (2020)

[52] ZHENG, Z. J., YU, J. L., LI, J. R., and LIN, J. Adhesive contact of power-law axisymmetric elastic objects. *Journal of University of Science and Technology of China*, **37**, 1293–1299 (2007)
[53] ZHU, Y. D., ZHENG, Z. J., ZHANG, Y. L., WU, H. G., and YU, J. L. Adhesion of elastic wavy surfaces: interface strengthening/weakening and mode transition mechanisms. *Journal of the Mechanics and Physics of Solids*, **151**, 104402 (2021)
[54] SONG, Z. and KOMVOPOULOS, K. Adhesion-induced instabilities in elastic and elastic-plastic contacts during single and repetitive normal loading. *Journal of the Mechanics and Physics of Solids*, **59**(4), 884–897 (2011)
[55] JIN, F., GUO, X., and GAO, H. J. Adhesive contact on power-law graded elastic solids: the JKR-DMT transition using a double-Hertz model. *Journal of the Mechanics and Physics of Solids*, **61**(12), 2473–2492 (2013)
[56] BIOT, M. A. Surface instability of rubber in compression. *Applied Scientific Research, Section A*, **12**(2), 168–182 (1963)
[57] YU, C. L., ZENG, W. J., WANG, B. J., CUI, X. W., GAO, Z. D., YIN, J., LIU, L. Q., WEI, X. L., WEI, Y. G., and DAI, Z. H. Stiffer is stickier: adhesion in elastic nanofilms. *Nano Letters*, **25**(5), 1876–1882 (2025)
[58] YUAN, W. K. and WANG, G. F. Adhesion between a rigid sphere and a stretched membrane using the Dugdale model. *International Journal of Solids and Structures*, **208-209**, 214–220 (2021)
[59] CIAVARELLA, M., GREENWOOD, J. A., and BARBER, J. R. Effect of Tabor parameter on hysteresis losses during adhesive contact. *Journal of the Mechanics and Physics of Solids*, **98**, 236–244 (2017)
[60] SONG, Z. and KOMVOPOULOS, K. Adhesive contact of an elastic semi-infinite solid with a rigid rough surface: strength of adhesion and contact instabilities. *International Journal of Solids and Structures*, **51**(6), 1197–1207 (2014)
[61] FENG, J. Q. Adhesive contact of elastically deformable spheres: a computational study of pull-off force and contact radius. *Journal of Colloid and Interface Science*, **238**(2), 318–323 (2001)

Appendix A

Here, we introduce the numerical method briefly. An effective finite integration interval [0, 10] is selected, beyond which the surface interaction becomes negligible[36,40]. The integral interval is uniformly divided into N segments ($[\rho_{i-1}, \rho_i]$) by $N+1$ nodes. Besides $\rho_0 = 0$, the remaining N nodes are located at $\rho_i\,(i = 1, 2, 3, \cdots, N)$ with surface separation $H_i = H(\rho_i)$. The values of $H_i\,(i = 1, 2, 3, \cdots, N)$ are determined by solving a system of nonlinear residual equations $R_i = 0$. From Eq. (21), R_i is defined as follows:

$$R_i = H_i - H_0 - \frac{1}{2}\rho_i^2 + \frac{16}{3}(\mu_{\mathrm{mod}})^{3/2}\rho_i \sum_{j=1}^{N}\Big(\Big(\frac{1}{H(\xi_j)+1}\Big)^3 - \Big(\frac{1}{H(\xi_j)+1}\Big)^9\Big)(\Psi(\rho_j/\rho_i) - \Psi(\rho_{j-1}/\rho_i)), \tag{A1}$$

where $H(\xi_j) = (H_{j-1} + H_j)/2$, and the Riemann-Stieltjes integration is employed. For a given H_0, Eq. (A1) is solved using the Newton-Raphson method. The iterative formulation is

$$(H_i^{(k+1)}) = (H_i^{(k)}) - (J_{ij}^{(k)})^{-1} R_i^{(k)}, \tag{A2}$$

where k denotes the iteration step, and (J_{ij}) represents the Jacobian matrix defined by $\frac{\partial R_i}{\partial H_j}$.

The iteration converges when both the maximum of $|(H_i^{(k+1)} - H_i^{(k)})/H_i^{(k)}|$ and the Euclidean norm of residual R_i are less than 10^{-6}. Once convergence is achieved, the normalized displacement A and the normalized load $P/(\pi\Delta\gamma R)$ can be calculated from the converged values of H_i as

$$A = -H(0) - \frac{16}{3}(\mu_{\mathrm{mod}})^{3/2}\sum_{j=1}^{N}\Big(\Big(\frac{1}{H(\xi_j)+1}\Big)^3 - \Big(\frac{1}{H(\xi_j)+1}\Big)^9\Big)(\rho_j - \rho_{j-1}), \tag{A3}$$

$$\frac{P}{\pi\Delta\gamma R} = -\frac{8}{3}\sum_{j=1}^{N}\Big(\Big(\frac{1}{H(\xi_j)+1}\Big)^3 - \Big(\frac{1}{H(\xi_j)+1}\Big)^9\Big)(\rho_j^2 - \rho_{j-1}^2). \tag{A4}$$